References

1. Mekontso Dessap A, Boissier F, Charron C, Bégot E, Repessé X, Legras A, *et al.* Acute cor pulmonale during protective ventilation for acute respiratory distress syndrome: prevalence, predictors, and clinical impact. *Intensive Care Med* 2016;42:862–870.
2. COVID-ICU Group on behalf of the REVA Network and the COVID-ICU Investigators. Clinical characteristics and day-90 outcomes of 4244 critically ill adults with COVID-19: a prospective cohort study. *Intensive Care Med* 2021;47:60–73.
3. Hewitt N, Bucknall T, Faraone NM. Lateral positioning for critically ill adult patients. Cochrane Database Syst Rev 2016(5):CD007205.
4. Jardin F, Dubourg O, Guéret P, Delorme G, Bourdarias J-P. Quantitative two-dimensional echocardiography in massive pulmonary embolism: emphasis on ventricular interdependence and leftward septal displacement. *J Am Coll Cardiol* 1987;10:1201–1206.
5. Belenkie I, Dani R, Smith ER, Tyberg JV. Ventricular interaction during experimental acute pulmonary embolism. *Circulation* 1988;78:761–768.
6. Riad Z, Mezidi M, Subtil F, Louis B, Guérin C. Short-term effects of the prone positioning maneuver on lung and chest wall mechanics in patients with acute respiratory distress syndrome. *Am J Respir Crit Care Med* 2018;197:1355–1358.
7. Nakao S, Come PC, Miller MJ, Momomura S, Sahagian P, Ransil BJ, *et al.* Effects of supine and lateral positions on cardiac output and intracardiac pressures: an experimental study. *Circulation* 1986;73:579–585.
8. Li Bassi G, Panigada M, Ranzani OT, Zanella A, Berra L, Cressoni M, *et al.*; Gravity-VAP Network. Randomized, multicenter trial of lateral Trendelenburg versus semirecumbent body position for the prevention of ventilator-associated pneumonia. *Intensive Care Med* 2017;43:1572–1584.
9. Evrard B, Goudelin M, Fedou A-L, Vignon P. Hemodynamic response to prone ventilation in COVID-19 patients assessed with 3D transesophageal echocardiography. *Intensive Care Med* 2020;46: 2099–2101.
10. Guérin C, Reignier J, Richard J-C, Beuret P, Gacouin A, Boulain T, *et al.*; PROSEVA Study Group. Prone positioning in severe acute respiratory distress syndrome. *N Engl J Med* 2013;368:2159–2168.

Cyclosporin A Reveals Potent Antiviral Effects in Preclinical Models of SARS-CoV-2 Infection

To the Editor:

Betacoronaviruses readily infect humans and cause pandemic outbreaks once new variants emerge from zoonotic reservoirs, such as severe acute respiratory syndrome coronavirus (SARS-CoV) in 2002–2003, Middle East respiratory syndrome coronavirus (MERS-CoV) in 2012, and severe acute respiratory syndrome coronavirus 2 (SARS-CoV-2) in 2019. Coronavirus disease (COVID-19) is characterized by an early oligosymptomatic phase with high viral replication in the upper respiratory tract that may progress to pneumonia, respiratory failure, and a severe systemic inflammatory response, causing more than 4 million deaths worldwide to date. Despite ongoing vaccination programs, effective and readily available drugs are still needed, considering the high number of those unvaccinated or the rapidly waning immunity in some risk groups, together with novel immune escape variants. Currently available broadly antiinflammatory treatment options such as corticosteroids (1) or additional IL-6R antagonists are applied in severe COVID-19, but for the latter, trial results regarding mortality are conflicting (2, 3). The only SARS-CoV-2 antiviral that has been applied routinely in humans, remdesivir, failed to reduce 28-day mortality in the Solidarity trial and is no longer recommended by the World Health Organization (4).

Combining antiviral and immunomodulatory effects, the immunophilin inhibitor cyclosporin A (CsA) is a promising candidate for the treatment of different CoVs. CsA is a U.S. Food and Drug Administration–approved immunosuppressive drug in medical use since 1983 to prevent graft-versus-host disease after organ transplant. CsA blocks the peptidyl-prolyl *cis-trans* isomerase activity of cyclophilins mediating diverse cellular processes (e.g., protein folding) (5). Protein–protein interaction screens revealed that cyclophilins are direct interaction partners of the SARS-CoV nonstructural protein 1, highlighting cyclophilins as important targets for antivirals. Accordingly, CsA was found to block replication of different viruses, including CoVs, *in vitro* (6). In an attempt to decipher the putative mode of action, we recently revealed that CsA, despite its known immunosuppressive actions in T lymphocytes, elicits a potent antiviral immune response by inducing IFN regulatory factor 1–dependent IFN-lambda (type III IFN) release, resulting in IFN-stimulated gene–dependent antiviral reprogramming of the lung epithelium and preservation of barrier function after MERS-CoV infection *in vitro* and *in vivo* (7). Moreover, a retrospective observational study of patients with COVID-19 treated with CsA demonstrated a significant mortality decrease (8).

Here, we demonstrate that CsA acts as a potent antiviral against different SARS-CoV-2 isolates in translational *in vitro*/*ex vivo* and *in vivo* models. Human bronchial epithelial cells (HBEpCs) of six different donors fully differentiated under air–liquid interface conditions for at least 21 days were infected with SARS-CoV-2 (BavPat1/2020 isolate, European Virus Archive Global 026V-03883, München-1.1/2020/929; termed "wild type" [WT]), resulting in significant replication with viral particle release into the medium of the apical compartment. CsA (10 μM) did not reveal substantial cytotoxicity in this model (not shown) and reduced SARS-CoV-2 *E* gene expression and viral titers significantly compared with control (Figures 1A and 1B). We then used donor lung–derived precision-cut lung slices (PCLSs) that were viable in *ex vivo* culture after sectioning for up to 14 days for infection with SARS-CoV-2 WT and CsA or DMSO treatment. Of note, SARS-CoV-2 replicated efficiently in PCLSs (9). SARS-CoV-2 *E* gene expression was quantified in homogenates together with viral titers in supernatant. Application of CsA significantly reduced virus titers in the medium and *E* gene RNA compared with DMSO-treated control (Figures 1C and 1D);

Supported by the Deutsche Forschungsgemeinschaft (KFO309 projects P2 and P8 to S.H. and S.B. [project number 284237345]; SFB-TR84 project B2 and B9 to S.H. [project number 114933180], SFB1021 project C5 to S.H. [project number 197785619], EXC2026 to S.H. [project number 390649896]). A.B. received grants from the Fraunhofer-Institut für Zelltherapie und Immunologie Drug Repurposing for Corona. L.S. and S.B. were supported by the Von-Behring-Röntgen-Stiftung (project number 68-0003). S.H. and S.B. were funded by the Pandemienetzwerk Hessen and the Netzwerk Universitätsmedizin (COVIM Project).

Originally Published in Press as DOI: 10.1164/rccm.202108-1830LE on February 15, 2022

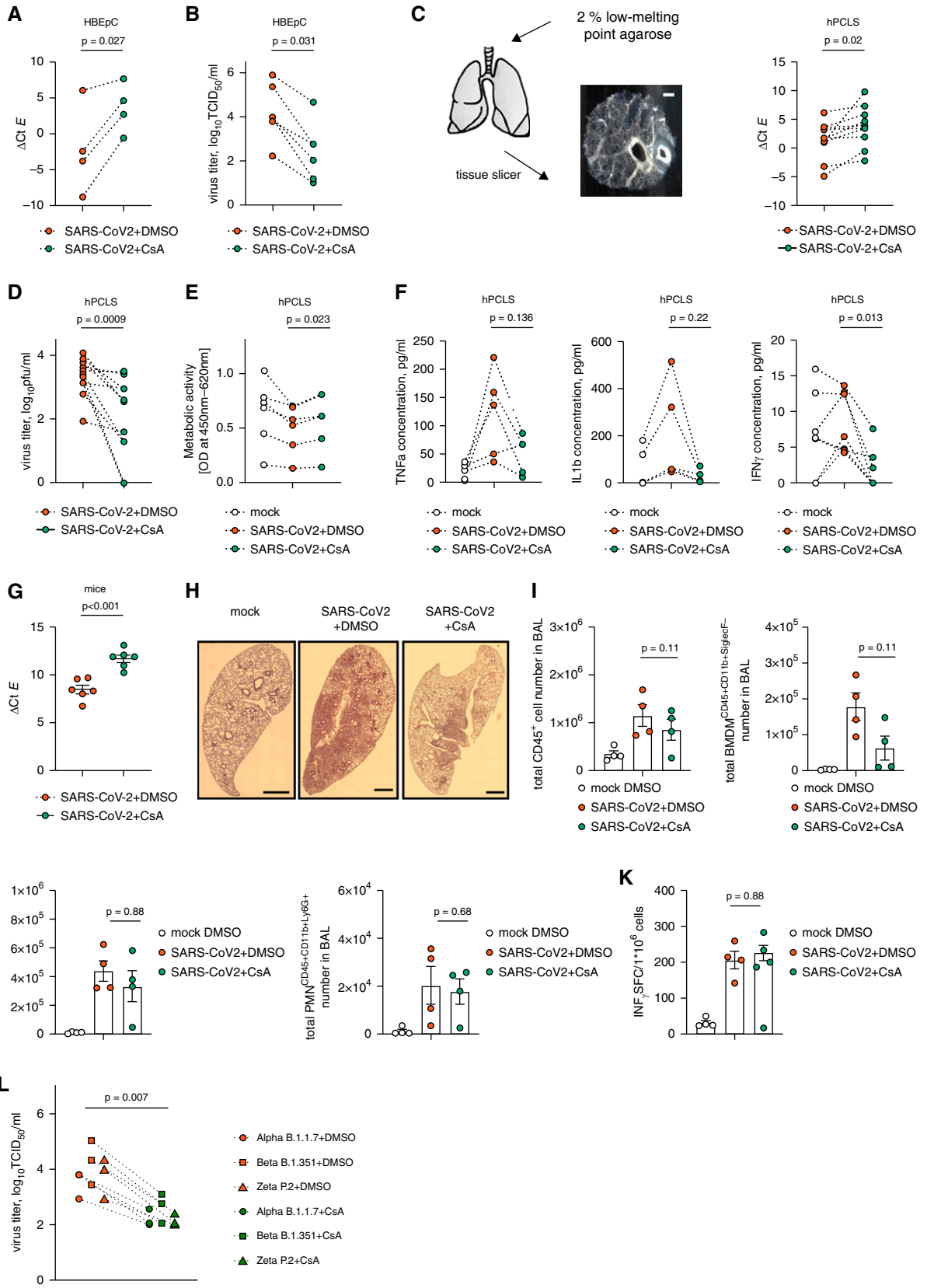

Figure 1. Cyclosporin A (CsA) counteracts severe acute respiratory syndrome coronavirus 2 (SARS-CoV-2) infection in human cells, lung tissue, and mice. (*A* and *B*) Fully differentiated human bronchial epithelial cells (HBEpCs) from four to six different donors were infected with

recovered metabolic activity of PCLSs (Figure 1E), indicating preservation of functional tissue integrity; and decreased proinflammatory cytokine concentration (tumor necrosis factor-α, $P = 0.136$; IL-1b, $P = 0.22$; and IFN-γ, $P = 0.013$) in supernatant of infected PCLSs (Figure 1F), indicating that CsA exerts immunomodulatory functions either directly or as a consequence of decreased viral replication. We next adapted our established MERS-CoV infection mouse model to analyze the effect of CsA *in vivo* by transducing Balb/c mice with orotracheally applied adenoviral vector encoding for human angiotensin-converting enzyme 2/mCherry, resulting in high expression levels of the human receptor in the lung epithelium ([7] and not shown). Mice were fed daily with CsA or DMSO solved in a chocolate creme for 6 days at a dose that reached serum concentration levels equal to those achieved in patients receiving oral CsA treatment (7). Three days after transduction, we infected mice with SARS-CoV-2 WT and analyzed viral load (*E* gene) in infected lung homogenates by quantitative PCR. CsA treatment resulted in efficient reduction of viral RNA in infected mice compared with control animals (Figure 1G).

Correspondingly, CsA-treated mice revealed reduced cell infiltration in lung tissue (Figure 1H) that was mainly reflected by a decrease in recruitment of bone marrow–derived macrophages (quantified in BAL; $P = 0.11$) (Figures 1I and 1J) that were found to significantly contribute to the imbalanced, hyperinflammatory immune response in severe COVID-19 (10, 11), whereas neutrophil recruitment was unaffected (Figure 1J). Given the reduced release of IFN-γ in SARS-CoV-2–infected PCLSs after CsA treatment, we aimed to rule out that CsA blunts antigen-specific T cell responses. As shown in Figures 1J and 1K, neither the total number of T cells in BAL nor the number of spike protein–specific splenic T cells was affected by CsA, suggesting that the adaptive immune response toward SARS-CoV-2 was maintained even after systemic CsA treatment in mice.

Given the indirect, host response–dependent mode of action of CsA (involving an IFN regulatory factor 1–IFN-lambda [type III IFN] signaling axis) that we recently identified (7), we speculated that CsA would be similarly active against newly emerging variants of concern or variants of interest that display different sets of mutations increasing viral fitness and transmission rates or providing immune escape (12). Vaccinated humans are protected against most upcoming variants; nevertheless, often a reduced antibody recognition of the mutated spike protein of these variants is detectable compared with original SARS-CoV-2 WT (12). We comparatively analyzed the effect of CsA against three different SARS-CoV-2 strains: variant of concern-α (UK variant, B 1.1.7), variant of concern-β (B1.351), and variant of interest zeta (Brazil variant, Zeta/P.2) in HBEpCs. HBEpCs were efficiently infected with all three isolates, and CsA blocked viral release of the three isolates, suggesting sustained efficacy in variants that harbor adaptive mutations (Figure 1L).

Figure 1. (*Continued*). SARS-CoV-2 (BavPat1/2020 isolate, European Virus Archive Global 026V-03883) at a multiplicity of infection (MOI) of 0.1 and stimulated with CsA (10 μM) or DMSO (control). Twenty-four hours after infection (p.i.), (*A*) expression of the SARS-CoV-2 *E* gene was analyzed by quantitative PCR (qPCR), and (*B*) release of infectious viral particles was determined by 50% tissue culture–infective dose ($TCID_{50}$) assay. As a normalization control for qPCR, the level of cellular 18S ribosomal (18S) rRNA was used. Graphs display single values for each donor. Statistical significance was calculated using a paired Student's *t* test for qPCR and the Wilcoxon signed-rank test for the $TCID_{50}$ assay. (*C–F*) Human precision-cut lung slices (hPCLSs), obtained by Krumdieck tissue slicer cut from 2% (wt/vol) low-melting-point agarose-filled resected human lungs from 10 or 11 different donors who underwent lobectomy, were infected with SARS-CoV-2 and stimulated with CsA (10 μM) or DMSO. Seventy-two hours p.i., (*C*) expression of the SARS-CoV-2 *E* gene was analyzed by qPCR, (*D*) release of infectious viral particles was determined by plaque assay, and (*E*) metabolic activity as a determinant of tissue integrity was analyzed by water soluble tetrazolium (WST)-1 assay (based on conversion of tetrazolium salt to formazan by mitochondrial dehydrogenases of viable cells, performed according to the manufacturer's protocol). (*F*) Cytokine concentrations in PCLS supernatant were determined by Bio-Plex assay according to the manufacturer's protocol 24 hours p.i. for TNFa (tumor necrosis factor-α) and IL-1b and 72 h p.i. for IFN-γ. As a normalization control for qPCR, the level of cellular 18S rRNA was used. Graphs represent single values for each donor: $n = 10$ for qPCR, $n = 11$ for plaque assay, $n = 6$ for WST-1 assay, and $n = 5–7$ for Bio-Plex assay. Statistical significance was calculated using a paired Student's *t* test for qPCR and the Wilcoxon signed-rank test for plaque assay, and pairwise comparisons were made by one-way ANOVA with Tukey's multiple comparisons test. Photomicrograph in *C* depicts a PCLS. Scale bar, 100 μm. (*G*) Balb/c mice were intratracheally infected with recombinant adenovirus encoding for human angiotensin-converting enzyme 2 (Ad-hACE2). Oral application of CsA (50 mg/kg/d) or DMSO (control) was started at Day 1 after transduction, followed by intranasal infection with 1.5×10^4 $TCID_{50}$/ml SARS-CoV-2 at Day 3 after transduction. Mice were killed 4 days after SARS-CoV-2 infection, total RNA was isolated from lung homogenate, and viral RNA (*E* gene) per 18S was measured by qPCR. Bar graphs represent single ΔCt values ± SEM; $n = 6$. Statistical significance was calculated using an unpaired Student's *t* test. (*H–J*) Mice were intratracheally transduced with recombinant adenovirus Ad-hACE2, followed by oral application of CsA (50 mg/kg/d) or DMSO (control) and by infection with SARS-CoV-2. Mice were killed 7 days after SARS-CoV-2 infection. (*H*) The left lung lobe was extracted, fixed, and embedded in paraffin, and tissue sections were stained with hematoxylin and eosin. BAL was collected before left lung lobe extraction. (*I* and *J*) Single-cell suspension was stained with combinations of antibody against the following markers and subjected to flow cytometric analysis: allophycocyanin (APC)–cyanine 7 anti-CD45, fluorescein isothiocyanate (FITC) anti-CD3, APC anti-Ly6G, BV421 anti-Siglec F, and FITC anti-CD11b. Graphs represent absolute number of indicated cell populations in BAL. Pairwise comparisons were made by Mann-Whitney *U* test. Scale bar, 1,000 μm. (*K*) Mice were transduced, infected, and treated as described above, and antigen-specific T cell numbers were quantified by IFN-γ enzyme-linked immunospot assay from splenocytes stimulated with SARS-CoV-2 spike peptides. Graph represents mean ± SEM; $n = 4$. Pairwise comparisons were made by Mann-Whitney *U* test. (*L*) HBEpCs were infected with either α (B.1.1.7 variant, BioProject no. PRJNA721582), β (B.1.351), or zeta (P.2, GenBank accession no. MW822593) SARS-CoV-2 variant at an MOI of 0.1 and stimulated with CsA (10 μM) for 24 h. The amount of released infectious viral particles was measured by $TCID_{50}$ assay. Bar graphs in represent mean ± SEM; $n = 3$. Statistical significance was calculated using the Wilcoxon signed-rank test. BMDM = bone marrow–derived macrophage; ΔCt = the difference in the threshold cycles of E gene and housekeeping gene 18S; OD = optical density; pfu = plaque forming unit; PMN = polymorphonuclear neutrophil; SFC = spot-forming cells.

Taken together, we used several preclinical, human-relevant infection models to expand our findings on the antiviral actions of CsA against MERS-CoV (7) to SARS-CoV-2 and emerging variants. These results highlight the pan-CoV inhibitory effect of CsA in human-relevant models and suggest CsA as potent antiviral, likely most effective when applied early after initial infection in humans. Some questions, however, remain regarding its putative antiviral effects beyond those that we described in MERS-CoV infection (7, 13) and whether and how its immunomodulatory effects would additionally impact COVID-19 courses.

Liposomal CsA for local (inhalational) deposition was found to be safe without systemic side effects and is currently applied in clinical trials (www.ClinicalTrials.gov identifier NCT03657342). Inhalational use of this drug early in the infection course to combat SARS-CoV-2 replication and therefore to prevent severe COVID-19 would be a cost-effective and readily available antiviral therapy with eventual additional benefits for the misbalanced pulmonary inflammation driven by macrophages (10). A phase II trial testing the effect of inhaled liposomal CsA (L-CsA-i) in patients recently diagnosed with SARS-CoV-2 infection is therefore underway (EudraCT 2021-004020-15). ■

Author disclosures are available with the text of this letter at www.atsjournals.org.

Acknowledgment: The authors acknowledge Sandra Ciesek, Christian Keller, and the European Virus Archive Global for providing virus isolates; Larissa Hamann, Florian Lück, Nadine Biedenkopf, and Helena Müller for experimental support; and Jochen Wilhelm for the help with statistical analysis.

Lucie Sauerhering, Ph.D.*
Philipps University of Marburg
Marburg, Germany
and
German Center for Infection Research
Braunschweig, Germany

Irina Kuznetsova, Ph.D.*
University of Giessen
Giessen, Germany

Alexandra Kupke, Ph.D.
Lars Meier, M.Sc.
Sandro Halwe, Ph.D.
Cornelius Rohde, M.Sc.
Jörg Schmidt
Philipps University of Marburg
Marburg, Germany

Rory E. Morty, Ph.D.
University of Giessen
Giessen, Germany
and
German Center for Lung Research
Giessen, Germany

Olga Danov, Ph.D.
Armin Braun, Ph.D.
Fraunhofer Institute for Toxicology and Experimental Medicine
Hannover, Germany
and
German Center for Lung Research
Giessen, Germany

István Vadász, M.D.
University of Giessen
Giessen, Germany

Institute for Lung Health
Giessen, Germany
and
German Center for Lung Research
Giessen, Germany

Stephan Becker, Ph.D.‡
Philipps University of Marburg
Marburg, Germany
and
German Center for Infection Research
Braunschweig, Germany

Susanne Herold, M.D., Ph.D.‡§
University of Giessen
Giessen, Germany

Institute for Lung Health
Giessen, Germany

German Center for Lung Research
Giessen, Germany
and
German Center for Infection Research
Braunschweig, Germany

ORCID IDs: 0000-0001-5487-3243 (L.S.); 0000-0001-8517-4779 (A.K.); 0000-0002-4021-7728 (S. Halwe); 0000-0002-4752-8326 (C.R.); 0000-0003-0833-9749 (R.E.M.); 0000-0001-6860-5610 (O.D.); 0000-0002-1142-1463 (A.B.); 0000-0003-1370-9783 (I.V.); 0000-0001-6343-0911 (S. Herold).

*Shared first authorship.
‡Shared senior authorship.
§Corresponding author (e-mail: susanne.herold@innere.med.uni-giessen.de).

References

1. Horby P, Lim WS, Emberson JR, Mafham M, Bell JL, Linsell L, *et al.*; RECOVERY Collaborative Group. Dexamethasone in hospitalized patients with Covid-19. *N Engl J Med* 2021;384:693–704.
2. Gordon AC, Mouncey PR, Al-Beidh F, Rowan KM, Nichol AD, Arabi YM, *et al.*; REMAP-CAP Investigators. Interleukin-6 receptor antagonists in critically ill patients with Covid-19. *N Engl J Med* 2021;384:1491–1502.
3. Salama C, Han J, Yau L, Reiss WG, Kramer B, Neidhart JD, *et al.* Tocilizumab in patients hospitalized with Covid-19 pneumonia. *N Engl J Med* 2021;384:20–30.
4. Pan H, Peto R, Henao-Restrepo AM, Preziosi MP, Sathiyamoorthy V, Abdool Karim Q, *et al.*; WHO Solidarity Trial Consortium. Repurposed antiviral drugs for Covid-19 — interim WHO Solidarity trial results. *N Engl J Med* 2021;384:497–511.
5. Harikishore A, Yoon HS. Immunophilins: structures, mechanisms and ligands. *Curr Mol Pharmacol* 2015;9:37–47.
6. Pfefferle S, Schöpf J, Kögl M, Friedel CC, Müller MA, Carbajo-Lozoya J, *et al.* The SARS-coronavirus-host interactome: identification of cyclophilins as target for pan-coronavirus inhibitors. *PLoS Pathog* 2011; 7:e1002331.
7. Sauerhering L, Kupke A, Meier L, Dietzel E, Hoppe J, Gruber AD, *et al.* Cyclophilin inhibitors restrict Middle East respiratory syndrome coronavirus *via* interferon-λ *in vitro* and in mice. *Eur Respir J* 2020;56: 1901826.

8. Guisado-Vasco P, Valderas-Ortega S, Carralón-González MM, Roda-Santacruz A, González-Cortijo L, Sotres-Fernández G, *et al.* Clinical characteristics and outcomes among hospitalized adults with severe COVID-19 admitted to a tertiary medical center and receiving antiviral, antimalarials, glucocorticoids, or immunomodulation with tocilizumab or cyclosporine: a retrospective observational study (COQUIMA cohort). *EClinicalMedicine* 2020;28:100591.
9. Hoffmann M, Hofmann-Winkler H, Smith JC, Krüger N, Arora P, Sørensen LK, *et al.* Camostat mesylate inhibits SARS-CoV-2 activation by TMPRSS2-related proteases and its metabolite GBPA exerts antiviral activity. *EBioMedicine* 2021;65:103255.
10. Grant RA, Morales-Nebreda L, Markov NS, Swaminathan S, Querrey M, Guzman ER, *et al.*; NU SCRIPT Study Investigators. Circuits between infected macrophages and T cells in SARS-CoV-2 pneumonia. *Nature* 2021;590:635–641.
11. Knoll R, Schultze JL, Schulte-Schrepping J. Monocytes and macrophages in COVID-19. *Front Immunol* 2021;12:720109.
12. Harvey WT, Carabelli AM, Jackson B, Gupta RK, Thomson EC, Harrison EM, *et al.*; COVID-19 Genomics UK (COG-UK) Consortium. SARS-CoV-2 variants, spike mutations and immune escape. *Nat Rev Microbiol* 2021;19:409–424.
13. de Wilde AH, Zevenhoven-Dobbe JC, van der Meer Y, Thiel V, Narayanan K, Makino S, *et al.* Cyclosporin A inhibits the replication of diverse coronaviruses. *J Gen Virol* 2011;92:2542–2548.

Population Prevalence of Hypercapnic Respiratory Failure from Any Cause

To the Editor:

Hypercapnic respiratory failure (HRF) is a severe sequela of many respiratory, cardiovascular, metabolic, and neurological diseases, yet there are no data on its prevalence at a population level. Previous studies are limited to reporting the prevalence of HRF as a complication of specific diseases, such as chronic obstructive pulmonary disease (COPD). However, this approach fails to recognize alternative diagnoses that contribute to the burden of disease associated with HRF. Furthermore, patients with COPD and HRF may have other conditions, such as sleep-disordered breathing, congestive cardiac failure, and obesity, which contribute to "multifactorial" HRF (1). In the setting of aging demography and multimorbidity, we believe better understanding of the population-level epidemiology of HRF is required to assist planning of health services and to provide context for future research on optimal management. Some of the following results have been previously reported in abstract form (2, 3).

Supported by funding from the Respiratory, Sleep, Environmental and Occupational Health (RSEOH) Group of Maridulu Budyari Gumal (Sydney Partnership for Health, Education, Research and Enterprise).

Author Contributions: Conception and design: Y.C., G.B.M., and H.V. Analysis and interpretation: Y.C., F.L.G., G.B.M., and H.V. Drafting the manuscript for important intellectual content: Y.C., F.L.G., G.B.M., and H.V.

Originally Published in Press as DOI: 10.1164/rccm.202108-1912LE on January 27, 2022

To estimate the 12-month period prevalence of HRF (including acute, chronic, and acute-on-chronic HRF) at a population level, we conducted a cross-sectional study of adults aged 15 or more years living in Liverpool, Australia, a large metropolitan area in southwestern Sydney. Cases were defined as members of the source population who attended Liverpool Hospital from January 1, 2013, to December 31, 2017, whose first arterial blood gas (ABG) sample taken within 24 hours of presentation revealed $Pa_{CO_2} > 45$ mm Hg and pH ≤ 7.45. We excluded blood gas results in which the Sa_{O_2} was at least 10% lower than the pulse oximetry Sp_{O_2}, as these were assumed to be venous specimens. We also excluded potentially nosocomial cases, defined as those in which the person had suffered an out-of-hospital cardiac arrest, traumatic injury, or if the specimen was collected during or shortly after a procedure requiring general anesthesia and/or sedation. We multiplied counts in each age stratum by the inverse of the proportion of persons in the source population who attended Liverpool Hospital for respiratory conditions, to account for underenumeration due to attendance at other hospitals. From Ministry of Health data, we ascertained that, on average, 86% of the source population who were hospitalized for respiratory conditions presented to Liverpool Hospital (4). This proportion ranged from 73% to 91% in the lowest and highest age strata, respectively. Age- and sex-specific mid-year population estimates were obtained from the Australian Bureau of Statistics (5). Average adjusted annual period prevalence rates and 95% confidence intervals (CI) were determined based on Poisson regression with the logarithm of 100,000 person-years as the offset term. Further regressions were performed to determine the associations between age group, sex, and their interaction on HRF prevalence. All analyses were performed in SAS (version 9.4; SAS Institute Inc.).

During the 5-year study period, we identified 2018 ABG records that met initial screening criteria. After excluding 144 probable venous specimens and 739 potential nosocomial cases, we found 1,135 episodes of HRF, attributable to 891 unique persons. Mean (SD) age was 69 (17) years, and 50.4% were males. Acidosis (pH < 7.35) was present in 488 (55%) cases. The average adjusted annual period prevalence of HRF during the study period was 163 (95% CI, 154–172) cases per 100,000 population.

HRF prevalence increased with age, from 14 (95% CI, 9–22) cases per 100,000 population for the age group 15–24 years, to 1,712 (95% CI, 1481–1,981) cases per 100,000 population for those aged 85 years or more (Table 1). Compared with those aged 45–54 years, each successive decade of life conferred increases in HRF prevalence by 2.1, 6.2, 15.7, and 26.2 times ($P < 0.0001$). There was no significant difference in HRF prevalence between males and females overall. However, among those less than 55 years of age, the prevalence rate of HRF among men was 4.4 (95% CI, 1.8–10.7) times that among women ($P = 0.02$).

Our study confirms that the population prevalence of HRF, estimated at 163 cases per 100,000 population, is substantially higher than previously estimated in studies limited to patients with COPD. A large study of COPD-related acidosis conducted in 1997 in the United Kingdom reported standardized yearly rates of 57 and 75 cases per 100,000 population for women and men aged 45–79 years, respectively (6). The comparatively high prevalence observed in this study may be attributable to an increase in COPD prevalence over time (7) but more likely reflects the importance of other conditions as contributors to the burden of HRF. This